Tribol Lett (2014) 55:23–33
DOI 10.1007/s11249-014-0328-x

ORIGINAL PAPER

Transient Heat Conduction Between Rough Sliding Surfaces

Yuwei Liu · J. R. Barber

Received: 6 January 2014 / Accepted: 31 March 2014 / Published online: 10 April 2014

Abstract When two rough bodies slide against each other, asperities on the opposing surfaces interact with each other, defining a transient contact and heat conduction problem. We represent each body by a Greenwood and Williamson asperity model with a Gaussian height distribution of identical spherical asperities. The heat transfer during a typical asperity interaction is analyzed, and the results are combined with the height distributions to determine the mean heat flux and the mean normal contact pressure as functions of the separation between reference planes in the two surfaces. We find that the effective thermal conductance is an approximately linear function of nominal contact pressure, but it also increases with the square root of the sliding speed and decreases with the 3/4 power of the combined RMS roughness. The results can be used to define an effective thermal contact resistance and division of frictional heat in macroscale (e.g., finite element) models of engineering components, requiring as input only the measured roughness and material properties.

Keywords Heat conduction · Sliding contacts · Rough surfaces

List of symbols

a	Contact radius
a_0	Maximum contact radius
A_{nom}	Nominal contact area
b	Nearest approach
b_0	Maximum value of b for contact
d	Maximum interference
d_0	See Eq. (5)
D	Fractal dimension of the profile
E^*	Composite elastic modulus
h_i	Asperity height above a datum
h_0	Mean plane separation
k	Thermal diffusivity
K	Thermal conductivity
$m_{0,2,4}$	Moments of the power spectral density
N_i	Surface density of summits
p	Contact pressure
P	Normal contact force
Pe	Peclet number
q	Heat flux per unit area
Q	Total heat transfer
R_i	Radius of asperity summit
R^*	Composite radius
S	Sliding distance
t	Time
t_0	Half of the duration of contact
T_i	Bulk temperatures
T_0	Flash temperature
$\bar{T}_0$	Average flash temperature
V	Relative velocity
x, y	Cartesian coordinates
α	Bandwidth parameter
θ	Temperature difference $T_1 - T_2$
ϕ_i	Height distribution of asperities
Φ_i	Probability distribution for asperity interaction
μ	Coefficient of friction
σ_i	Summit height standard deviation
ω_h	Upper cut-off frequency

Y. Liu
School of Mechanical Engineering, Beijing Institute of Technology, Beijing 100081, China
e-mail: yuweiliu1@gmail.com

Y. Liu · J. R. Barber (✉)
Department of Mechanical Engineering, University of Michigan, Ann Arbor, MI 48109-2125, USA
e-mail: jbarber@umich.edu

Subscripts and superscripts

c	Heat flux due to temperature difference
f	Heat generated by friction
$i = 1, 2$	Bodies 1, 2
nom	Nominal contact

1 Introduction

When two bodies slide against each other, frictional heat is generated at the interface. Since all practical surfaces are rough on the microscale, contact is restricted to areas of actual contact between surface asperities and these contacts are also the location of the frictional heating, leading to high local 'flash temperatures' [1]. However, in the analysis of real engineering systems—for example using the finite element method—it is not generally possible to model the details of the surface topography and appropriate 'averaged' boundary conditions must be assumed at the interface. The usual convention is to assume temperature continuity at the interface, but this is clearly unrealistic since the imperfect contact imposes a resistance to heat flow and is known to cause the 'bulk temperature' [essentially the average temperature at the interface or on a plane slightly below the interface] to differ between the two contacting bodies [2, 3].

The resistance to heat flow between stationary [non-sliding] contacting rough surfaces is a mature subject of research, and generally, it is found that the conductance [reciprocal of resistance] is approximately proportional to the nominal contact pressure [4], though many numerical and analytical models predict power-law dependence significantly different from linearity [5], as do experimental results [6]. However, these results cannot be carried over to the sliding contact problem, since the relative motion has a major effect on the heat conduction problem.

Early models of the sliding contact problem were developed by Blok [7] and Jaeger [8] and extended to more general contact areas by Bos and Moes [9]. All these authors assumed that (1) the typical contact area is sustained long enough for a steady thermal state to be established, (2) the contact area is fixed in one body and sliding over the other, and (3) the two bodies can be represented as half spaces whose temperatures at infinity are zero—in other words, the bulk temperatures in the two bodies are equal. The results depend heavily on the 'Peclet number' $Pe = Va/k$, where V is the sliding velocity, a is a typical dimension of the contact area, and k is the thermal diffusivity of the material. When $Pe \gg 1$, which is typically the case in tribological applications, most of the frictional heat passes into the 'moving' body and hardly any into the stationary body, meaning the body on which the contact area is fixed, unless the moving body has a much lower thermal conductivity.

The kinematic assumptions (1, 2) are appropriate if one body is smooth, or if asperities on a rough hard body plough through a smoother softer body. Of course, it is traditional in contact mechanics to define a fictitious rough body combining the roughness of the two contacting surfaces, but in the case of sliding, this changes the problem qualitatively. If both surfaces are rough, the typical asperity interaction will be transient with a short time scale, and it is unrealistic to expect a thermal steady state to be established [10, 11]. Furthermore, the kinematics is now symmetrical about the interfacial plane [12] and in the absence of a bulk temperature difference, the frictional heat partition for similar materials would be equal, even at high Peclet number [13]. We also note that the sliding contact of two rough surfaces is necessarily stochastic, with contact occurring at different parts of the surfaces at different times, leading to dynamic effects and a stochastic distribution of flash temperatures [14, 15].

In this paper, we shall represent each of the rough surfaces by classical asperity models and investigate the statistics of the asperity interactions during sliding and the resulting heat exchange. Notice in particular that the typical interaction involves asperity pairs passing near but not exactly over each other's summits and the contact period at each interaction, and hence the heat exchange, will depend on the nearest approach distance as well as the asperity heights. The results will enable us to estimate the effective thermal conductance between the sliding surfaces and in particular to explore the dependence of this quantity on roughness and material parameters as well as on the nominal contact pressure and sliding speed.

2 Transient Contact of an Asperity Pair

Following Greenwood and Williamson [16], we represent each rough surface as a distribution of spherical asperities of various heights. The typical mechanical and thermal interaction will be a transient process in which an asperity on body 2 passes sufficiently close to an asperity on body 1 to experience a period of contact.

Figure 1 shows a plan view of this process. We can assume without loss of generality that body 1 is stationary and that body 2 moves to the right at a constant velocity V. The point A_1 identifies the location of the summit of an asperity in body 1 with radius R_1 and height h_1 above some datum located in body 1. The point A_2 defines the instantaneous position of the summit of an asperity in body 2 of radius R_2 and height h_2 relative to a datum in body 2. As body 2 moves, the point A_2 traces out the dashed horizontal line in Fig. 1, whose nearest approach to A_1 is denoted by b. We choose to define time t such that $t = 0$ at the point of nearest approach, so that at other times, the x-coordinate of A_2 is Vt.

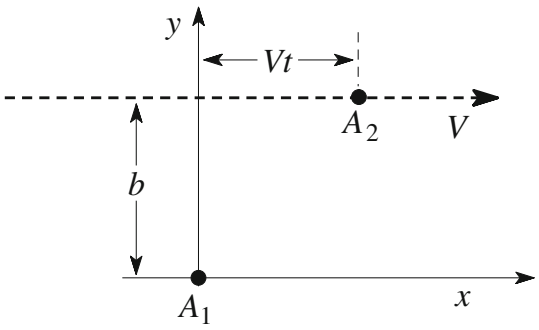

Fig. 1 Trajectory of the summit A_2 of asperity 2. The summit of asperity 1 is stationary at A_1

If the bodies are located such that the distance between the datum planes in the two bodies is h_0, the contact problem can be defined by an 'interference function'

$$f(x,y) = h_1 + h_2 - h_0 - \frac{x^2+y^2}{2R_1} - \frac{(x-Vt)^2+(y-b)^2}{2R_2}, \tag{1}$$

representing the local value of interpenetration of the surfaces if this were not prevented by contact forces. Moving the origin of coordinates by defining

$$x = \xi + \frac{R_1 Vt}{(R_1+R_2)}; \quad y = \eta + \frac{R_1 b}{(R_1+R_2)}, \tag{2}$$

we obtain

$$f(\xi,\eta) = d_0 - \frac{(Vt)^2}{2(R_1+R_2)} - \frac{\xi^2+\eta^2}{2R^*}, \tag{3}$$

where

$$d_0 = h_1 + h_2 - h_0 - \frac{b^2}{2(R_1+R_2)}; \quad \frac{1}{R^*} = \frac{1}{R_1} + \frac{1}{R_2}. \tag{4}$$

It is convenient to write the first of these equations as

$$d_0 = \frac{b_0^2 - b^2}{2(R_1+R_2)} \quad \text{where} \quad b_0 = \sqrt{2(R_1+R_2)(h_1+h_2-h_0)} \tag{5}$$

is the maximum value of b for which the interaction involves contact. The maximum interference occurs at $\xi = \eta = 0$ and is given by

$$d = d_0\left(1 - \frac{t^2}{t_0^2}\right) \quad \text{where} \quad t_0 = \frac{\sqrt{2d_0(R_1+R_2)}}{V}. \tag{6}$$

Contact occurs while $d > 0$ and hence $-t_0 < t < t_0$. When this condition is satisfied, Eq. (3) defines an axisymmetric Hertzian contact problem for which the radius a of the contact area, the normal contact force P and the contact pressure distribution $p(r)$ are given by [17]

$$a = \sqrt{R^* d}; \quad P = \frac{4E^*\sqrt{R^*}d^{3/2}}{3};$$
$$p(r) = \frac{2E^*}{\pi}\sqrt{\frac{d}{R^*}\left(1 - \frac{r^2}{a^2}\right)}. \tag{7}$$

2.1 The Heat Conduction Problem

Since the roughness of the surfaces is to be explicitly described by an asperity model, the bodies will be within the range of interatomic forces in regions of actual contact, so we assume continuity of temperature (perfect thermal contact) in these regions. The duration $2t_0$ of a typical asperity interaction event will be extremely small, so it is reasonable to assume that the bulk temperatures remain constant and that the heat conduction problem is dominated by conduction in the direction perpendicular to the contact surface [18]. In other words, lateral conduction can be neglected, which reduces the problem to a single space coordinate and time. In particular, if two stationary bodies with thermal conductivity K_i and thermal diffusivity k_i, and initially uniform temperatures T_i, $i = 1, 2$ are brought into perfect thermal contact for a short period Δt, the total heat flux per unit area into each body during the contact will be [18, 19]

$$q_1 = \frac{C_1 q_f}{(C_1+C_2)} - \frac{2C_1C_2\theta}{(C_1+C_2)}\sqrt{\frac{\Delta t}{\pi}};$$
$$q_2 = \frac{C_2 q_f}{(C_1+C_2)} + \frac{2C_1C_2\theta}{(C_1+C_2)}\sqrt{\frac{\Delta t}{\pi}}, \tag{8}$$

where $C_i = K_i/\sqrt{k_i}$, $\theta = T_1 - T_2$, and q_f is the total heat generated per unit area at the interface during the contact.

The asperity contact problem is complicated by the relative motion, which causes a given point on body 1 to make contact with a range of points on body 2 during the interaction. For example, Fig. 2a shows the extent of the contact area on body 1 at various instants during the interaction for the case where $R_1 = R_2$ and we notice that as the circular contact area grows and then shrinks, it also moves. Here, we shall make the simplifying assumption that the contact radius varies in the same way in time [given by Eqs. (6, 7), but without relative motion, as shown in Fig. 2b. We shall estimate the error due to this approximation in Appendix 1.

2.1.1 Frictional Heating

The total frictional heat generated during the asperity interaction is given by

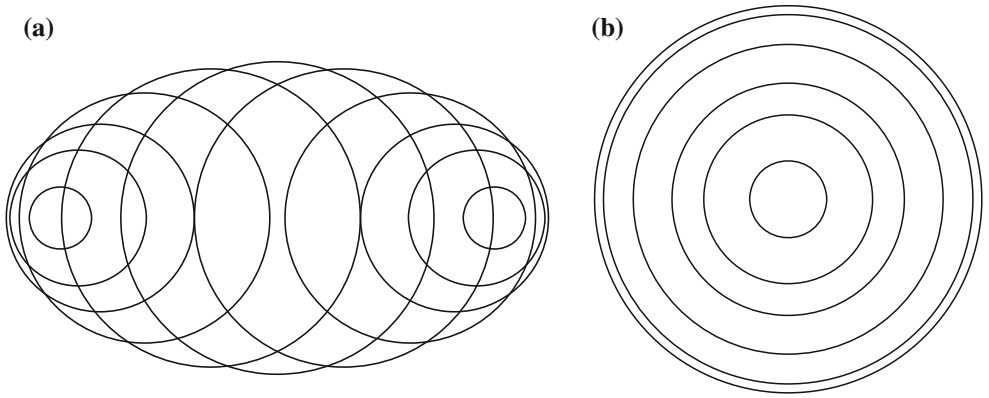

Fig. 2 **a** Contact area at various instants during the interaction; **b** simplified kinematics used in the analysis

$$Q_f = \int_{-t_0}^{t_0} \mu P(t) V \mathrm{d}t = \frac{4\mu V E^* \sqrt{R^*} d_0^{3/2}}{3} \int_{-t_0}^{t_0} \left(1 - \frac{t^2}{t_0^2}\right)^{3/2} \mathrm{d}t$$
$$= \frac{\pi \mu E^* \sqrt{R_1 R_2} d_0^2}{\sqrt{2}} = \frac{\pi \mu E^* \sqrt{R_1 R_2} (b_0^2 - b^2)^2}{4\sqrt{2}(R_1 + R_2)^2}, \quad (9)$$

after substituting for t_0, d_0 from Eqs. (5, 6), respectively, where μ is the friction coefficient which is assumed to be independent of pressure and velocity.

Equation (8) shows that in the absence of a temperature difference θ, the frictional heat will be distributed between the two bodies in the fixed ratio C_1/C_2, giving a total heat flow into bodies 1 and 2 of

$$Q_f^{(1)} = \frac{C_1 Q_f}{(C_1 + C_2)}; \quad Q_f^{(2)} = \frac{C_2 Q_f}{(C_1 + C_2)}. \quad (10)$$

Notice that these results are appropriate when the asperity interactions are of short duration, and hence, sliding speeds are high. At very slow sliding speeds, a thermal steady state will be established and the frictional heat will be partitioned in the ratio of conductivities K_1/K_2 [15].

2.1.2 Heat Exchange Due to a Temperature Difference θ

We next consider the modification to these results due to the existence of a temperature difference θ between the two bodies. From Eqs. (6, 7), we conclude that a point at radius r will experience contact as long as $r < a(t)$ and hence for a period

$$\Delta t = 2t_0 \sqrt{1 - \frac{r^2}{a_0^2}} \quad \text{where} \quad a_0 = \sqrt{R^* d_0} \quad (11)$$

is the maximum radius of the contact circle. Substituting this result into Eq. (8) and integrating over the contact area, we find the total heat flux from body 1 into body 2 due to the temperature difference θ alone is

$$Q_c = \frac{4C_1 C_2 \theta \sqrt{2\pi t_0}}{(C_1 + C_2)} \int_0^{a_0} \left(1 - \frac{r^2}{a_0^2}\right)^{1/4} r \mathrm{d}r = \frac{8 C_1 C_2 \theta a_0^2 \sqrt{2\pi t_0}}{5(C_1 + C_2)}. \quad (12)$$

Substituting for t_0, a_0, d_0 from Eqs. (5, 6, 11), respectively, we then obtain

$$Q_c = A_c (b_0^2 - b^2)^{5/4} \quad \text{where} \quad A_c = \frac{4\sqrt{2\pi} C_1 C_2 \theta R^*}{5(C_1 + C_2)(R_1 + R_2)\sqrt{V}}. \quad (13)$$

The kinematic approximation illustrated in Fig. 2b will tend to underestimate the heat exchanged between the bodies for a given value of the temperature difference θ. The exact calculation is generally intractable, but it can be performed for the special case where $C_2 \gg C_1$, and this provides a method of estimating the error introduced by the approximation of Fig. 2b. This analysis is given in Appendix 2, and it shows that for the case where the asperities on the two surfaces have the same summit radius [$R_1 = R_2$], Eq. (13) underestimates the heat exchange by a factor of $\sqrt[4]{3} \approx 1.32$. Notice that this is a purely numerical factor. The parametric dependence of the heat exchange on sliding speed, and roughness parameters is unchanged by the kinematic approximation of Fig. 2b.

2.1.3 Flash Temperature

Although the focus in this paper is on the macroscopic heat transfer behavior resulting from microscopic asperity interactions, we also record here the maximum temperature resulting from the frictional heating defined in Eq. (9). With the simplified kinematics of Fig. 2b, this will occur at the center of the contact area $r = 0$, where the frictional heating rate per unit area is

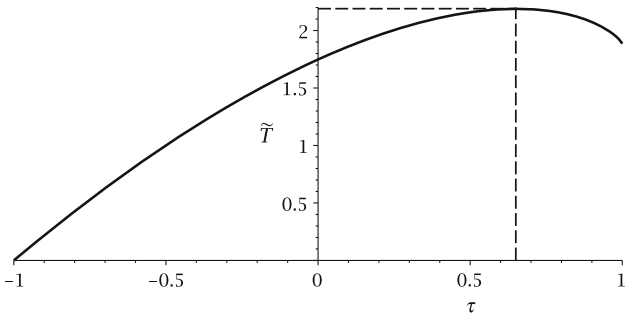

Fig. 3 Variation of dimensionless central temperature $\tilde{T}(\tau)$ during a single asperity interaction

$$q_0(t) = \mu V p(0) = \frac{2\mu V E^*}{\pi}\sqrt{\frac{d_0}{R^*}(1-\tau^2)}, \tag{14}$$

from Eqs. (6, 7), where $\tau = t/t_0$. The temperature at this point can then be obtained as

$$T_0(t) = \int_{-t_0}^{t} \frac{q_0(s)\mathrm{d}s}{(C_1+C_2)\sqrt{\pi(t-s)}} = \frac{2\mu V E^*}{(C_1+C_2)\pi^{3/2}}\sqrt{\frac{d_0 t_0}{R^*}}\tilde{T}(\tau) \tag{15}$$

where the dimensionless integral

$$\tilde{T}(\tau) = \int_{-1}^{\tau}\sqrt{\frac{1-\zeta^2}{\tau-\zeta}}\mathrm{d}\zeta \tag{16}$$

is plotted in Fig. 3. A similar variation of temperature during a transient interaction was obtained by Smith and Arnell [12] (see their Fig. 3) using a finite element model. The maximum value occurs at $\tau = 0.65$ and is 2.19, so the maximum (flash) temperature is given by

$$T_0 = \frac{4.38\mu V E^*}{(C_1+C_2)\pi^{3/2}}\sqrt{\frac{d_0 t_0}{R^*}} = \frac{0.94\mu\sqrt{V}E^*(R_1+R_2)^{3/4}d_0^{3/4}}{(C_1+C_2)\sqrt{R_1 R_2}}, \tag{17}$$

after substituting for t_0 from $(6)_2$.

3 Statistics of Asperity Interactions

The Greenwood and Williamson (GW) asperity model [16], comprises a set of N_i identical spherical asperities per unit nominal area of summit radius R_i, randomly distributed in the interfacial plane and following a Gaussian height distribution with standard deviation σ_i. This model is very idealized, since for example, asperities are generally not axisymmetric and higher summits have larger mean curvatures [20]. However, McCool [21] compared the GW model with less restrictive models and showed that it is nonetheless surprisingly accurate in its predictions.

3.1 Determination of GW Parameters

According to Nayak [20], a random and isotropic surface with a homogeneous, Gaussian height distribution can be adequately characterized by the three moments (m_0), (m_2), (m_4) of the power spectral density function. These values can be determined from a profile function $z(x)$ as

$$m_0 = \left\langle z(x)^2 \right\rangle; \quad m_2 = \left\langle z'(x)^2 \right\rangle; \quad m_4 = \left\langle z''(x)^2 \right\rangle, \tag{18}$$

where $z(x)$ represents the profile height deviation from an arbitrary datum plane at some position x and can be derived from a profilometer or AFM. The square root of m_0 is the RMS roughness of the surface, m_2 is the mean square slope, and m_4 is the mean square curvature.

The GW parameters N_i, R_i can then be obtained from the spectral moments as [22]

$$N_i = \frac{1}{6\pi\sqrt{3}}\frac{(m_4)_i}{(m_2)_i}; \quad R_i = \frac{3}{8}\sqrt{\frac{\pi}{(m_4)_i}}, \tag{19}$$

and Bush et al. [23] express the summit height standard deviation σ_i, as

$$\sigma_i = \left(1 - \frac{0.8968}{\alpha_i}\right)^{1/2}\sqrt{(m_0)_i}, \tag{20}$$

where

$$\alpha_i = \frac{(m_0)_i(m_4)_i}{(m_2)_i^2} \tag{21}$$

is the bandwidth parameter. As $\alpha_i > 1.5$ [20], Eq. (20) shows that the summits have lower variance than the surface as a whole—i.e. $\sigma_i < \sqrt{(m_0)_i}$, but the difference is small and reduces as α_i becomes large.

It is more usual in tribology to use the profile mean plane as a reference, rather than the summit mean plane used by the GW model [22], but since the plane separation will be used merely as an intermediate step in determining relations between macroscopic quantities, we here use the more convenient GW definition.

3.2 Probability of a Single Interaction

Suppose that each surface contains only a single asperity, and we wish to determine the probability distribution $\Phi(b)$ of an asperity interaction occuring during sliding through a distance S, where b is the nearest approach of the asperities

shown in Fig. 1. The distribution $\Phi(b)$ is defined such that the probability of an interaction between b and $b+\delta b$ is $\Phi(b)\delta b$. Since the location of the asperities is random, we can determine this probability by fixing the location A_1 of the asperity in body 1 and covering the entire nominal area A_{nom} by a set of parallel lines separated by a small distance δb, representing the trajectory of A_2. The total length of these lines is $A_{\text{nom}}/\delta b$ and just two of them lie in the required range (one on each side of A_1), so the required probability function is $2S/A_{\text{nom}}$. However, since there are N_1 asperities on surface 1 and N_2 on surface 2 per unit nominal area, the probability distribution for asperity interactions is given by

$$\Phi(b) = 2SN_1N_2A_{\text{nom}}. \tag{22}$$

3.3 Asperity Height Distributions

The frictional heat generated Q_f and the heat transferred between the bodies Q_c at each asperity interaction depends on d_0 through Eqs. (9, 13) and hence on the heights h_1, h_2 of the respective asperities through Eq. (4). We assume a Gaussian distribution of asperities with height, so that the probability of a given asperity on surface i having a height between h_i and $h_i+\delta h_i$ is $\phi(h_i)\delta h_i$ where

$$\phi_i(h_i) = \frac{1}{\sqrt{2\pi}\sigma_i}\exp\left(-\frac{h_i^2}{2\sigma_i^2}\right). \tag{23}$$

3.4 Total Frictional Heat Generated

Each asperity interaction results in the generation of an amount of frictional heat Q_f given by Eq. (9), so the total frictional heat generated per unit nominal area when sliding a distance S can be obtained by integrating with respect to h_1, h_2, b, giving

$$Q_f(S) = \frac{1}{A_{\text{nom}}}\int_{-\infty}^{\infty}\int_{h_0-h_2}^{\infty}\int_{0}^{b_0}\Phi(b)\phi(h_1)\phi_2(h_2)Q_f\text{dbdh}_1\text{dh}_2, \tag{24}$$

where b_0 is given by Eq. (5). This integral is evaluated in Appendix 1 and can be written

$$Q_f(S) = \frac{2^{21/4}N_1N_2\sqrt{\pi}E^*\sqrt{R_1+R_2}\sqrt{R_1R_2}\mu S\left(\sigma_1^2+\sigma_2^2\right)^{5/4}}{15} I_f(\hat{h}_0), \tag{25}$$

where

$$I_f(\hat{h}_0) = \int_0^{\infty} e^{-(y+\hat{h}_0)^2}y^{5/2}\text{dy} \quad \text{and} \quad \hat{\text{h}}_0 = \frac{\text{h}_0}{\sqrt{2(\sigma_1^2+\sigma_2^2)}}. \tag{26}$$

This integral can be expressed in terms of special functions using (for example) Maple or Mathematica.

3.5 Heat Exchange Due to a Temperature Difference

An exactly similar procedure can be used to determine the total heat exchanged between the bodies due to a bulk temperature difference θ. We simply replace Q_f by Q_c in Eq. (24), obtaining

$$Q_c(S) = \frac{1}{A_{\text{nom}}}\int_{-\infty}^{\infty}\int_{h_0-h_2}^{\infty}\int_{0}^{b_0}\Phi(b)\phi(h_1)\phi_2(h_2)Q_c\text{dbdh}_1\text{dh}_2, \tag{27}$$

where Q_c is given by Eq. (13).

This integral is evaluated in Appendix 2 and can be written

$$Q_c(S) = \frac{2^{45/8}\pi^{3/2}SN_1N_2C_1C_2\theta R_1R_2(\sigma_1^2+\sigma_2^2)^{7/8}}{21\Gamma(3/4)^2(C_1+C_2)(R_1+R_2)^{1/4}\sqrt{V}} I_c(\hat{h}_0), \tag{28}$$

where

$$I_c(\hat{h}_0) = \int_0^{\infty} e^{-(y+\hat{h}_0)^2}y^{7/4}\text{dy}. \tag{29}$$

3.6 The Nominal Heat Flux

The velocity V is the distance S slid per unit time, and hence the rate of heat generation per unit nominal area due to friction is obtained by replacing S by V in Eq. (25), giving

$$q^f_{\text{nom}} = \frac{2^{21/4}N_1N_2\sqrt{\pi}E^*\sqrt{R_1+R_2}\sqrt{R_1R_2}\mu V\left(\sigma_1^2+\sigma_2^2\right)^{5/4}}{15} I_f(\hat{h}_0). \tag{30}$$

Similarly, the nominal heat flux from body 1 to body 2 due to a temperature difference $\theta = (T_1 - T_2)$ is

$$q^c_{\text{nom}} = \frac{2^{45/8}\pi^{3/2}N_1N_2C_1C_2(T_1-T_2)R_1R_2(\sigma_1^2+\sigma_2^2)^{7/8}\sqrt{V}}{21\Gamma(3/4)^2(C_1+C_2)(R_1+R_2)^{1/4}} I_c(\hat{h}_0), \tag{31}$$

from (28). The heat flux into bodies 1 and 2 can then be obtained by superposition as

$$q_1 = \frac{C_1q^f_{\text{nom}}}{(C_1+C_2)} - q^c_{\text{nom}}; \quad q_2 = \frac{C_2q^f_{\text{nom}}}{(C_1+C_2)} + q^c_{\text{nom}}. \tag{32}$$

3.7 The Mean Nominal Pressure

If the mean separation h_0 is maintained constant, the normal force P, and hence, the nominal contact pressure $p_{\text{nom}} = P/A_{\text{nom}}$ will fluctuate randomly because of the statistical nature of the asperity interactions. However, the mean value must satisfy the equation

$$Q_f(S) = \mu p_{\text{nom}} S \tag{33}$$

since this represents the work done against friction during sliding through a distance S. Using this result and Eq. (25), we then obtain

$$p_{\text{nom}} = \frac{2^{21/4} N_1 N_2 \sqrt{\pi} E^* \sqrt{R_1 + R_2} \sqrt{R_1 R_2} \left(\sigma_1^2 + \sigma_2^2\right)^{5/4}}{15} I_f(\hat{h}_0). \tag{34}$$

3.8 Stochastic Distribution of Flash Temperatures

Since asperity interactions occur with a range of values of maximum interference d_0, the flash temperatures generated at these interactions will have a stochastic distribution [14, 15]. The present model enables us to estimate the statistical properties of this distribution.

We first determine the total number of interactions per unit nominal contact area when sliding a distance S, which is

$$N(h_0) = \frac{1}{A_{\text{nom}}} \int_{-\infty}^{\infty} \int_{h_0 - h_2}^{\infty} \int_{0}^{b_0} \Phi(b)\phi(h_1)\phi_2(h_2) \text{dbdh}_1 \text{dh}_2. \tag{35}$$

This integral can be evaluated using the same method as in Appendix 2 giving

$$N(h_0) = \frac{2^{7/4} N_1 N_2 \sqrt{R_1 + R_2} S \left(\sigma_1^2 + \sigma_2^2\right)^{1/4}}{\sqrt{\pi}} I\left(\hat{h}_0, \frac{1}{2}\right), \tag{36}$$

where $I(\hat{h}_0, \gamma)$ is an integral defined in Eq. (57).

Now, if the mean plane separation h_0 were increased by some value d_1, any interactions for which $d_0 < d_1$ would cease to occur, and the number of interactions would be decreased to $N(h_0 + d_1)$. It follows that the proportion of the interactions at h_0 that satisfy the condition $d_0 > d_1$ is

$$\frac{N(h_0 + d_1)}{N(h_0)} = \frac{I\left(\hat{h}_0 + \hat{d}_1, \frac{1}{2}\right)}{I\left(\hat{h}_0, \frac{1}{2}\right)}. \tag{37}$$

The flash temperature (17) is a monotonic function of d_0, so it follows that Eq. (37) also defines the probability that a given interaction will experience a flash temperature $T_0 > T_1$, where T_1 is obtained by substituting $d_0 = d_1$ in (17).

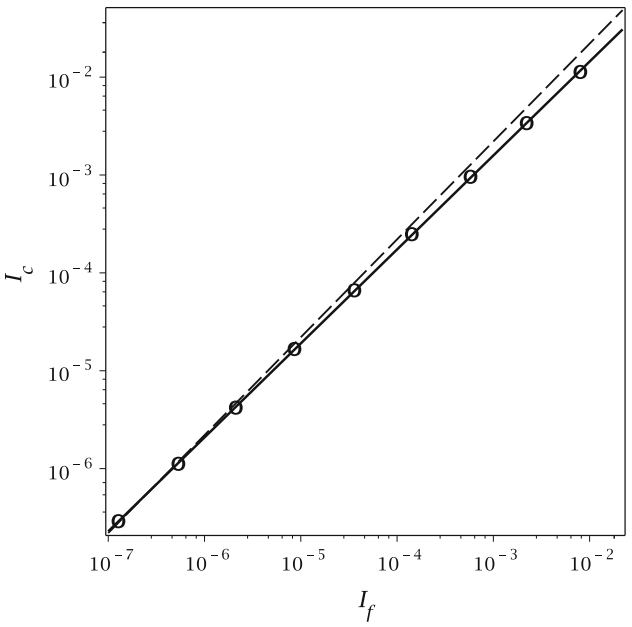

Fig. 4 The points represent the relationship between nominal heat flux q^c_{nom} and nominal contact pressure p_{nom} through the integrals I_c, I_f in Eqs. (31, 34). The *solid line* is the power-law fit (41), and the *dashed line* is the linear fit (42)

We can also determine the mean flash temperature as

$$\bar{T}_0 = \frac{1}{N(h_0) A_{\text{nom}}} \int_{-\infty}^{\infty} \int_{h_0 - h_2}^{\infty} \int_{0}^{b_0} \Phi(b)\phi(h_1)\phi_2(h_2) T_0 \text{dbdh}_1 \text{dh}_2, \tag{38}$$

where T_0 is defined in terms of d_0 and hence b through Eqs. (5, 17). Using the same methods as in Appendix 2, we obtain

$$\bar{T}_0 = \frac{0.87 \mu \sqrt{V} E^* (R_1 + R_2)^{3/4} \left(\sigma_1^2 + \sigma_2^2\right)^{3/8}}{(C_1 + C_2)\sqrt{R_1 R_2}} I_T, \tag{39}$$

where

$$I_T = \frac{I\left(\hat{h}_0, \frac{5}{4}\right)}{I\left(\hat{h}_0, \frac{1}{2}\right)}. \tag{40}$$

4 Results and Discussion

4.1 Thermal Contact Resistance

As the mean separation $\hat{h}_0$ is reduced, both the nominal pressure and the nominal heat flux q^c_{nom} due to the temperature difference $(T_1 - T_2)$ increase, but the dependence is not identical in the two expressions because of the different powers of y in the integrals (26) and (29). Figure 4 shows the relation between these integrals on a log-log scale and an almost perfect fit is provided by the straight line which corresponds to a power-law relation of the form

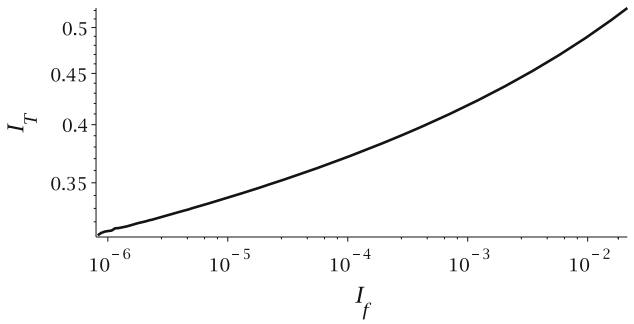

Fig. 5 Relation between average flash temperature $\bar{T}_0$ and nominal contact pressure p_{nom} through the integrals I_T, I_f in Eqs. (34, 40)

$$q^c_{\text{nom}} = B(T_1 - T_2)\sqrt{V}\, p^{0.96}_{\text{nom}}, \tag{41}$$

where B is a constant that depends upon the material and roughness parameters through Eqs. (31, 34).

Equation (41) shows that the thermal contact resistance is inverse with $V^{1/2}$. This results from the assumption that during sliding, the individual asperity interactions have very short duration and hence are unable to approach a thermal steady state, which is clearly not appropriate in the static limit $V \to 0$. Nonetheless, a very similar power exponent with pressure is generally obtained in the static case. For example, Mikic [24] (see also [25]) predicts an exponent of 0.94, though other authors report a weak dependence on fractal dimension [26].

The power law (41) is very close to linear and indeed in the range where the dimensionless mean separation $\hat{h}_0 > 2$ (which includes most practical contact situations) a very good linear fit can be obtained in the form

$$q^c_{\text{nom}} \approx \frac{4.26 C_1 C_2 \sqrt{R_1 R_2}(T_1 - T_2)\sqrt{V}}{(C_1 + C_2)(R_1 + R_2)^{3/4}(\sigma_1^2 + \sigma_2^2)^{3/8}} \frac{p_{\text{nom}}}{E^*}. \tag{42}$$

We should not be surprised to see nearly linear behavior here, since the original GW model (admittedly for a single rough surface contacting a plane) predicted near linearity for the relations between several other quantities that are sums over individual asperity events, notably normal load, electrical contact resistance, and total actual contact area [16]. The result follows from the assumed Gaussian distribution of asperity heights, which causes increases in load to be primarily accommodated by an increased number of actual contact areas, while leaving the size distribution relatively unchanged.

If the two sliding surfaces are identical, Eq. (42) reduces to

$$q^c_{\text{nom}} \approx \frac{0.98 K R^{1/4}(T_1 - T_2)\sqrt{V}}{\sqrt{k}\sigma^{3/4}} \frac{p_{\text{nom}}}{E^*}, \tag{43}$$

which has the advantage of exposing the dependence of the contstant of proportionality on the roughness parameters σ and R.

4.2 Average Flash Temperature

Figure 5 shows the average flash temperature $\bar{T}_0$ as a function of the nominal contact pressure p_{nom} represented through the integrals I_T, I_f, respectively, in Eqs. (34, 40). The average flash temperature increases modestly with increase in nominal pressure, but the dependence is very weak, amounting to only a 50 % increase over four decades increase in p_{nom}. This again is consistent with GW arguments.

Assuming an approximate value $I_T = 0.36$ and similar materials and surfaces, Eq. (39) predicts an average flash temperature of

$$\bar{T}_0 \approx \frac{0.34\mu\sqrt{kV}E^*\sigma^{3/4}}{KR^{1/4}}, \tag{44}$$

which shows a significant dependence on roughness amplitude and elastic modulus. It is interesting to note that the material and roughness parameters that affect $\bar{T}_0$ have an exactly inverse effect on the thermal contact resistance, so that Eqs. (43, 44) can be combined to yield the simple relation

$$\frac{q^c_{\text{nom}}}{(T_1 - T_2)} \approx \frac{\mu V p_{\text{nom}}}{3\bar{T}_0} \tag{45}$$

that is material and roughness independent.

4.3 Quasi-Fractal Surfaces

Many rough surfaces exhibit fractal characteristics, but a truly fractal surface would give unbounded values for the moments m_2, m_4. Theories of this kind therefore require that the spectral density be truncated at some upper cutoff frequency ω_h, and the usefulness of the results depends on the extent to which they depend on this essentially arbitrary parameter. In Eq. (43), this dependence results only from the term $R^{1/4}$, since σ is approximately independent of ω_h. Using Eq. (19), we then have

$$R^{1/4} \sim (m_4)^{-1/8} \sim \omega_h^{-D/4} \tag{46}$$

[27], where $D\,(1 \le D < 2)$ is the fractal dimension of the profile. The shortest wavelength of the truncated surface is $\lambda_h = 2\pi/\omega_h$ and a reasonable practical range for λ_h is between 10 nm and 10 μm, limited at the low end by the atomic structure of the material and at the high end by the requirement for an adequate description of the rough surface. Over this range, $R^{1/4}$ varies by a factor of $10^{-3D/4}$ which corresponds to 1/13 for $D = 1.5$, so the quantitative predictions of thermal contact resistance are significantly influenced by the roughness description chosen. However, the parametric dependence on material properties and

sliding speed and the approximately linear dependence on nominal pressure are independent of ω_h.

4.4 Application to Macroscale Finite Element Models

In a macroscale finite element model, the mesh is generally not sufficiently fine to describe the surface roughness, and indeed, the typical asperity interaction is likely to be several orders of magnitude smaller than the mesh dimension, so we can reasonably treat the bulk temperatures T_1, T_2 as surface nodal temperatures. We must therefore use averaged expressions for the heat fluxes at the sliding interface, and these values can be estimated from the results derived above.

We must first obtain or estimate the surface roughness parameters $R_1, R_2, \sigma_1, \sigma_2$ for substitution into Eq. (42). These are given in Sect. 3.1 in terms of properties of the surface profiles that can be obtained using profilometry. Alternatively, we note that σ_i is approximately equal to the RMS surface roughness which is likely to be specified in the design, and R_i appears only weakly in Eq. (42) [see (43)], so a rough estimate might reasonably be used.

The local heat fluxes q_1, q_2 into the two bodies in the macroscopic model are then given by Eq. (32) where $q^f_{\text{nom}} = \mu V p_{\text{nom}}$, q^c_{nom} is given by Eq. (42), and p_{nom} is the local contact pressure.

5 Conclusions

We have developed a Greenwood and Williamson model of sliding thermal contact to predict the average heat flux between two bodies at different temperatures and the average normal contact pressure, both as functions of the separation between mean planes in the respective surfaces. The model differs from most previous treatments of rough surface contact in that both surfaces are treated as rough, so the contact process is stochastic in both time and space, comprising a distribution of transient interactions between pairs of asperities. The transient nature of these interactions has a significant effect on the heat conduction problem.

We find that the effective thermal conductance is an approximately linear function of nominal contact pressure, but it also increases with the square root of the sliding speed and decreases with $\sigma^{3/4}$, where σ is the combined RMS roughness. The results can be used to define an effective thermal contact resistance and division of frictional heat in macroscale numerical models of engineering components, requiring as input only the measured roughness and material properties.

Appendix 1

Effect of Relative Motion

We consider the case where $C_2 \gg C_1$, so that points on the surface of body 2 can be assumed to remain at temperature T_2 throughout the contact, and for simplicity we assume that $R_1 = R_2 = R$—i.e. the asperities on the two surfaces have the same summit radius R.

A representative point (x, y) on the surface of body 1 will make contact as long as it remains within the appropriate contact circle in Fig. 2a—i.e. if $\xi^2 + \eta^2 \le a(t)^2$, where ξ, η and the time-varying contact radius $a(t)$ are defined in Eqs. (2, 7) respectively. Using these relations, the inequality can be written in terms of x, y, t as

$$\left(x - \frac{Vt}{2}\right)^2 + \left(y - \frac{b}{2}\right)^2 \le \frac{Rd_0}{2} - \frac{V^2 t^2}{8}, \tag{47}$$

and hence

$$\frac{3\tau^2}{2} - 2X\tau + X^2 + Y^2 - \frac{1}{2} \le 0, \tag{48}$$

where we define dimensionless time and coordinates through

$$X = \frac{x}{\sqrt{Rd_0}}; \quad Y = \frac{y}{\sqrt{Rd_0}} - \frac{b}{2\sqrt{Rd_0}}; \quad \tau = \frac{t}{t_0} = \frac{Vt}{2\sqrt{Rd_0}}. \tag{49}$$

The times τ_1, τ_2 at which contact begins and ends at a given point (X, Y) are defined by taking the equality in (48), giving

$$\tau_1, \tau_2 = \frac{2}{3}\left(X \mp \sqrt{\frac{3}{4} - \frac{X^2}{2} - \frac{3Y^2}{2}}\right). \tag{50}$$

It follows that the period of contact at this point is

$$\Delta\tau = \tau_2 - \tau_1 = \sqrt{\frac{4}{3}\left(1 - \frac{2X^2}{3} - 2Y^2\right)}. \tag{51}$$

Notice that by setting $\Delta\tau = 0$, we define the envelope of the contact regions in Fig. 2a, which is

$$\frac{2x^2}{3} + 2\left(y - \frac{b}{2}\right)^2 = Rd_0, \tag{52}$$

using (49). Points outside this ellipse never experience contact. The total heat exchanged per unit area at (X, Y) is given by Eq. (8) with $C_2 \to \infty$ as

$$q = 2C_1\theta\sqrt{\frac{\Delta t}{\pi}} = 2C_1\theta(Rd_0)^{1/4}\sqrt{\frac{2\Delta\tau}{\pi V}} = \frac{4C_1\theta(Rd_0)^{1/4}}{3^{1/4}\sqrt{\pi V}}\left(1-\frac{2X^2}{3}-2Y^2\right)^{1/4} \quad (53)$$

and hence the total heat exchange during the interaction is

$$Q_c = \int\int_{\mathcal{A}} q(x,y)dxdy = Rd_0\int\int_{\mathcal{A}} q(X,Y)\mathrm{dXdY}, \quad (54)$$

where the integration domain $\mathcal{A}$ comprises the ellipse of Eq. (52). We obtain

$$Q_c = \frac{8\sqrt[4]{3}C_1\sqrt{\pi}\theta(d_0R)^{5/4}}{5\sqrt{V}} = \frac{\sqrt[4]{3}C_1\sqrt{2\pi}\theta\left(b_0^2-b^2\right)^{5/4}}{5\sqrt{V}}, \quad (55)$$

which exceeds Eq. (13) [with $R_1 = R_2$] by a factor of $\sqrt[4]{3} \approx 1.32$.

Appendix 2

Evaluation of Gaussian Integrals

Consider the integral

$$J(\gamma) = \frac{1}{2\pi\sigma_1\sigma_2}\int_{-\infty}^{\infty}\int_{h_0-h_2}^{\infty}\exp\left(-\frac{h_1^2}{2\sigma_1^2}-\frac{h_2^2}{2\sigma_2^2}\right)(h_1+h_2-h_0)^{\gamma}\mathrm{dh_1dh_2}.$$

We define dimensionless parameters

$$x_1 = \frac{h_1}{\sigma_1\sqrt{2}}; \quad x_2 = \frac{h_2}{\sigma_2\sqrt{2}}$$

and then perform the linear transformation

$$\xi = \frac{x_1+\beta x_2}{\sqrt{1+\beta^2}}; \quad \eta = \frac{\beta x_1 - x_2}{\sqrt{1+\beta^2}} \quad \text{where} \quad \beta = \frac{\sigma_2}{\sigma_1}.$$

This preserves the condition

$$\xi^2+\eta^2 = x_1^2+x_2^2$$

so that the Jacobean of the transformation is unity. We also have

$$h_1+h_2-h_0 = (\xi-\hat{h}_0)\sqrt{2(\sigma_1^2+\sigma_2^2)} \quad \text{where} \quad \hat{h}_0 = \frac{h_0}{\sqrt{2(\sigma_1^2+\sigma_2^2)}},$$

and the domain of integration in $J(\gamma)$ is $\xi > \hat{h}_0$, giving

$$J(\gamma) = \frac{[2(\sigma_1^2+\sigma_2^2)]^{\gamma/2}}{\pi}\int_{\hat{h}_0}^{\infty}\int_{-\infty}^{\infty} e^{-(\xi^2+\eta^2)}(\xi-\hat{h}_0)^{\gamma}\mathrm{d}\eta\mathrm{d}\xi.$$

The integral with respect to η evaluates to $\sqrt{\pi}$ so that finally we obtain

$$J(\gamma) = \frac{[2(\sigma_1^2+\sigma_2^2)]^{\gamma/2}}{\sqrt{\pi}}I(\hat{h}_0,\gamma) \quad (56)$$

where

$$I(\hat{h}_0,\gamma) = \int_{\hat{h}_0}^{\infty} e^{-\xi^2}(\xi-\hat{h}_0)^{\gamma}\mathrm{d}\xi = \int_0^{\infty}\mathrm{e}^{-(\mathrm{y}+\hat{h}_0)^2}\mathrm{y}^{\gamma}\mathrm{dy}, \quad (57)$$

writing $y = \xi - \hat{h}_0$. The integral $I(\hat{h}_0,\gamma)$ can be evaluated in terms of special functions (for example using Mathematica or Maple) for integer and fractional values of γ.

Frictional Heating

Substituting $Q_f, \Phi(b), \phi_1(h_1), \phi_2(h_2)$ from Eqs. (9, 22, 23) respectively into Eq. (24), we obtain

$$Q_f(S) = \frac{SN_1N_2\pi\mu E^*\sqrt{R_1R_2}}{2\sqrt{2}(R_1+R_2)^2}I_1, \quad (58)$$

where

$$I_1 = \frac{1}{2\pi\sigma_1\sigma_2}\int_{-\infty}^{\infty}\int_{h_0-h_2}^{\infty}\int_0^{b_0}\exp\left(-\frac{h_1^2}{2\sigma_1^2}-\frac{h_2^2}{2\sigma_2^2}\right)(b_0^2-b^2)^2\mathrm{dbdh_1dh_2}$$

Evaluating the integral with respect to b and substituting for b_0 from (5), we have

$$I_1 = \frac{8[2(R_1+R_2)]^{5/2}}{15}J\left(\frac{5}{2}\right).$$

Substituting this result in (58) and using (56) we obtain

$$Q_f(S) = \frac{2^{21/4}N_1N_2\sqrt{\pi}E^*\sqrt{R_1+R_2}\sqrt{R_1R_2}\mu S\left(\sigma_1^2+\sigma_2^2\right)^{5/4}}{15}I\left(\hat{h}_0,\frac{5}{2}\right).$$

Heat Exchange Due to a Temperature Difference

Substituting $Q_c, \Phi(b), \phi_1(h_1), \phi_2(h_2)$ from Eqs. (13, 22, 23) respectively into Eq. (27), we obtain

$$Q_c(S) = \frac{2^{7/2}\pi SN_1N_2C_1C_2\theta R^*}{5(C_1+C_2)(R_1+R_2)\sqrt{\pi V}}I_2,$$

where

$$I_2 = \frac{1}{2\pi\sigma_1\sigma_2}\int_{-\infty}^{\infty}\int_{h_0-h_2}^{\infty}\int_{0}^{b_0}\exp\left(-\frac{h_1^2}{2\sigma_1^2}-\frac{h_2^2}{2\sigma_2^2}\right)$$
$$(b_0^2-b^2)^{5/4}\mathrm{dbdh_1dh_2}$$
$$=\frac{5\pi^{3/2}[2(R_1+R_2)]^{7/4}}{21\sqrt{2}\Gamma(3/4)^2}J\left(\frac{7}{4}\right)$$

after evaluating the integral with respect to b. We therefore have

$$Q_c(S)=\frac{2^{45/8}\pi^{3/2}SN_1N_2C_1C_2\theta R_1R_2(\sigma_1^2+\sigma_2^2)^{7/8}}{21\Gamma(3/4)^2(C_1+C_2)(R_1+R_2)^{1/4}\sqrt{V}}I\left(\hat{h}_0,\frac{7}{4}\right).$$

References

1. Archard, J.F.: The temperature of rubbing surfaces, Wear **2**, 438–455 (1958)
2. Ling, F.F., Simkins, T.E.: Measurement of pointwise juncture condition of temperature at the interface of two bodies in sliding contact. ASME J. Basic Eng. **85**, 481–487 (1963)
3. Bauzin, J.G., Laraqi, N.: Simultaneous estimation of frictional heat flux and two thermal contact parameters for sliding contacts. Numer. Heat Transf. A Appl. **45**, 313–328 (2004)
4. Persson, B.N.J., Lorenz, B., Volokitin, A.I.: Heat transfer between elastic solids with randomly rough surfaces. Eur. Phys. J. E **31**, 3–24 (2010). doi:10.1140/epje/i2010-10543-1
5. Bush, A.W., Gibson, R.D.: A theoretical investigation of thermal contact conductance. Appl. Energy **5**, 11–22 (1979)
6. Sridhar, M.R., Yovanovich, M.M.: Elastoplastic contact conductance model for isotropic, conforming rough surfaces and comparison with experiments. J. Heat Transf. **118**, 3–16 (1996)
7. Blok, H.: Theoretical study of temperature rise at surfaces of actual contact under oiliness conditions. Inst. Mech. Eng. Gen. Discuss. Lubr. **2**, 222–235 (1937)
8. Jaeger, J.C.: Moving sources of heat and the temperature of sliding contacts. J. Proc. R. Soc. N. S. W. **76**, 203–224 (1942)
9. Bos, J., Moes, H.: Frictional heating of tribological contacts. Trans. ASME J. Tribol. **117**, 171–177 (1995)
10. Gecim, B., Winer, W.O.: Transient temperatures in the vicinity of an asperity contact. Trans. ASME J. Tribol. **107**, 333–342 (1985)
11. Hou, Z.B., Komanduri, R.: General solutions for stationary/moving plane heat source problems in manufacturing and tribology. Int. J. Heat Mass Transf. **43**, 1679–1698 (2000)
12. Smith, E.H., Arnell, R.D.: A new approach to the calculation of flash temperatures in dry, sliding contacts. Tribol. Lett. **52**, 407–414 (2013)
13. Barber, J.R.: The distribution of heat between sliding surfaces. J. Mech. Eng. Sci. **9**, 351–354 (1967)
14. Ling, F.F., Pu, S.: Probable interface temperatures of solids in sliding contact. Wear **7**, 23–34 (1964)
15. Wang, S., Komvopoulos, K.: A fractal theory of the interfacial temperature distribution in the slow sliding regime: part I. Elastic contact and heat transfer analysis. J. Tribol. **116**, 812–823 (1994)
16. Greenwood, J.A., Williamson, J.B.P.: Contact of nominally flat surfaces. Proc. R. Soc. Lond. Ser. A **295**, 300–319 (1966)
17. Johnson, K.L.: Contact Mechanics. Cambridge University Press, Cambridge (1985)
18. Carslaw, H.S., Jaeger, J.C.: The Conduction of Heat in Solids, 2nd edn. Clarendon Press, Oxford (1959)
19. Incropera, F.P., DeWitt, D.P., Bergman, T.L., Lavine, A.S.: Fundamentals of Heat and Mass Transfer, 6th edn, pp. 283–289. Wiley, Manchester (2006)
20. Nayak, P.R.: Random process model of rough surfaces. ASME J. Lubr. Technol. **93**, 398–407 (1971)
21. McCool, J.I.: Comparison of models for the contact of rough surfaces. Wear **107**, 37–60 (1986)
22. McCool, J.I.: Relating profile instrument measurements to the functional performance of rough surfaces. Trans. ASME **109**, 264–270 (1987)
23. Bush, A.W., Gibson, R.D., Keogh, G.P.: The limit of elastic deformation in the contact of rough surfaces. Mech. Res. Commun. **3**, 169–174 (1976)
24. Mikic, B.B.: Thermal contact conductance: theoretical considerations. Int. J. Heat Mass Transf. **17**, 205–214 (1974)
25. Madhusudana, C.V.: Thermal Contact Conductance, 2nd edn, p. 32. Springer, New York (1996)
26. Paggi, M., Barber, J.R.: Contact conductance of rough surfaces composed of modified RMD patches. Int. J. Heat Mass Transf. **54**, 4664–4672 (2011)
27. Majumdar, A., Tien, C.L.: Fractal characterization and simulation of rough surfaces. Wear **136**, 313–327 (1990)